Polymer 159 (2018) 138–145

Contents lists available at ScienceDirect

Polymer

journal homepage: www.elsevier.com/locate/polymer

# Structure of block copolymer grafted silica nanoparticles

Vivek Goel[a], Joanna Pietrasik[b,c], Ryan Poling-Skutvik[a], Andrew Jackson[d,e], Krzysztof Matyjaszewski[c], Ramanan Krishnamoorti[a,f,*]

[a] Department of Chemical Engineering, University of Houston, Houston, TX, 77204, USA
[b] Department of Chemistry, Lodz University of Technology, Institute of Polymer and Dye Technology, 90 924, Lodz, Poland
[c] Department of Chemistry, Carnegie Mellon University, Pittsburgh, PA, 15213, USA
[d] NIST Center for Neutron Research, National Institute for Standards and Technology, Gaithersburg, MD, 20899-6102, USA
[e] Department of Materials Science and Engineering, University of Maryland, College Park, MD, 20742-2115, USA
[f] Department of Chemistry, University of Houston, Houston, TX, 77204, USA

## HIGHLIGHTS

- The morphology of a block copolymer of a near symmetric strongly-segregating poly(*n*-butyl acrylate) and poly(methyl methacrylate) tethered to a ~15 nm silica nanoparticles is examined.
- The copolymer components are strongly segregated and the nanoparticle hybrid forms a disordered structure that is a combination of coexisting individual randomly placed core-shell structures and worm-like cylinders with 3–5 silica nanoparticles forming the core of the cylinder.
- With increasing temperature, the cylinders become shorter.

## ARTICLE INFO

*Keywords:*
Nanoparticles
Block copolymers
Structure

## ABSTRACT

The morphology of a block copolymer of a near symmetric strongly-segregating poly(*n*-butyl acrylate) and poly (methyl methacrylate) tethered to a ~15 nm silica nanoparticles is examined using a combination of microscopy techniques and small angle x-ray and neutron scattering. The copolymer components are strongly segregated and form a disordered structure that is possibly a combination of coexisting individual randomly placed core-shell structures and worm-like cylinders with 3–5 silica nanoparticles forming the core. With increasing temperature, the cylinders become shorter because of the improved thermodynamic compatibility between the two copolymer segments.

## 1. Introduction

The use of nanoparticles to template and control the self-assembly of microphase separated block copolymers has proven to be attractive as nanoparticles can alter and mediate interactions between constituent polymers and provide a geometrical or topological effect that is significantly distinct from those afforded by addition of small molecule solvents and homopolymers or even block copolymers [1,2]. A comprehensive experimental study exploiting the thermodynamic interactions between nanoparticles and polymers to organize the nanoparticles in block copolymers was undertaken by Kramer and coworkers [3–9]. They used the ability to develop Janus spherical nanoparticles that, when incorporated into block copolymers, led to a placement of such nanoparticles in either microdomain or at the interface of the microdomains. Other experimental studies have indicated the ability of nanoparticles to alter the microdomain structure – for instance the addition of CdS spherical nanoparticles led to the transformation of cylindrical microdomains of poly(4-vinylpyridine) (to which the CdS nanoparticles can hydrogen bond) in polystyrene to transform to a lamellar microdomain system [10]. Separately, using molecular modeling, Jayaraman and coworkers [11] and Glotzer and coworkers [12,13] have shown the ability of nanoparticles to direct the assembly of tethered block copolymers to nanoscale structures not necessarily accessible through the untethered block copolymers or through the creation of equivalent triblock copolymers. Additionally, a study by Giannelis et al. indicated that the preferential interactions between layered silicates and the polystyrene block of a polystyrene-*b*-polyisoprene block copolymer could lead to some changes in the order-disorder transition, even though a thorough detailing of this was prevented by the changed transport properties of the chains due to the

* Corresponding author. Department of Chemical Engineering, University of Houston, Houston, TX, 77204, USA.
*E-mail address:* ramanan@uh.edu (R. Krishnamoorti).

https://doi.org/10.1016/j.polymer.2018.10.072
Received 25 August 2018; Received in revised form 27 October 2018; Accepted 30 October 2018
Available online 02 November 2018
0032-3861/ 

anisotropic silicate sheets [14].

On the other hand, the exploitation of the matching or mismatching of the geometry of the nanoparticle and the topology of the microphase separated structure of the block copolymer has been somewhat more extensively studied [1,10,15–22]. Studies utilizing silicate layers to reinforce lamellar block copolymers demonstrated that in spite of the nucleation tendencies of such materials, the overall effect of adding such nanoparticles was to significantly increase the defect density in such block copolymers [15]. On the other hand, using layered silicates of varying sizes, it has been shown that the smaller lateral dimension silicates can lead to a significant nucleation and templating of spherical block copolymers while largely leaving cylindrical microdomains to be unaffected by the addition of such nanoparticles [20]. Wiesner and coworkers have demonstrated the profound effect that filler dimensionality (spherical to rod-like to disc-like) has on the thermodynamic order-disorder transition of block copolymers [22].

The use of living polymerization methods from nanoparticle surfaces, the grafting-from process, has led to the ability to produce both homopolymers and block copolymers that are attached to nanoparticles [23–27]. These methods lead to the development of materials with controlled molecular weight and dispersity whose grafting density to the surface can be tailored by physical – chemical means and whose physical, mechanical and thermal properties can carefully tuned. Clearly, using nanoparticles with varying sizes (i.e., changing the inherent curvature imposed) and aspect ratios (spherical to rod-like to disc-like) from which polymers are grafted it is possible to systematically explore the effect of particle geometry on the morphological and phase behavior of block copolymers. The theoretical work over the last few years by Jayaraman, Riggleman, Kumar, Grest and Frischlmecht have provided tantalizing glimpses on the possibility of creating self-assembled structures [1,3–7,17,21].

In this paper, we describe the case of a poly(*n*-butyl acrylate)-*b*-poly (methyl methacrylate) grafted using atom transfer radical polymerization [28–30] from a ~15 nm spherical silica nanoparticles with a very high grafting density (~600 chains per nanoparticle). The block copolymer, if not attached to the nanoparticle, would result in the formation of a strongly segregated lamellae microdomain forming system (as indicated by the overall molecular weight and the roughly equal volume fraction composition of the material chosen) [31,32]. We specifically, describe detailed structural characterization of this block copolymer hybrid using a number of complementary techniques, including electron microscopy and small angle neutron and x-ray scattering.

## 2. Methods and materials

The monomers *n*-butyl acrylate (BA, Acros, 99%) and methyl methacrylate (MMA, Aldrich, 99%) were purified by filtration through a basic alumina column to remove inhibitors before synthesis [33]. The procedure for the synthesis of 1-(chlorodimethylsilyl)propyl 2-bromoisobutyrate and the subsequent functionalization of the silica (30 % wt. silica in methyl isobutyl ketone, effective diameter D = 16 nm, MIBK-ST, Nissan) was derived from previously described method [24]. Bis(2-pyridylmethyl)octadecylamine (BPMODA) was synthesized according to the literature [34]. CuBr and CuCl (Aldrich, 99%) were purified via several slurries in acetic acid followed by filtration and washing with methanol and ethyl ether, and stored under nitrogen before use. $CuBr_2$, $CuCl_2$ (Aldrich, 99.999%), polyoxyethylene (20) oleyl ether (Brij 98, Aldrich), hexadecane (Aldrich), L-ascorbic acid (AA, Aldrich, 99%), 4,4′-dinonyl-2,2′-dipyridyl (dNbpy, Aldrich, 97%), diphenyl ether (Fluka) and hydrofluoric acid (50 vol % HF, Acros) were used as received.

Poly(*n*-butyl acrylate) homopolymer brushes were synthesized by activators generated by electron transfer (AGET) ATRP [35–38] of BA from 2-bromoisobutyrate functionalized silica particles in miniemulsion under conditions similar to those reported previously, BA: $SiO_2$—Br: $CuBr_2$: BPMODA: ascorbic acid = 600: 1: 0.5: 0.5: 0.2, temperature 80 °C [18,39]. The polymerization of MMA from silica grafted poly(*n*-butyl acrylate) was carried out at 70 °C. $SiO_2$-*g*-PBA (0.8897 g, 0.0152 mmol Br), MMA (10 mL, 93 mmol), $CuCl_2$ (0.0010 g, 0.0076 mmol), dNbpy (0.1305 g, 0.3192 mmol) and DPE (1 mL) were added to a 25-mL Schlenk flask equipped with a magnetic stir bar. The flask was sealed, and the resulting solution was subjected to three freeze-pump-thaw cycles. After equilibration at room temperature, CuCl (0.0151 g, 0.1523 mmol) was added to the solution under nitrogen flow and the flask was placed in preheated oil bath. After a predetermined time, the flask was removed from the oil bath and opened to expose the catalyst to air. The polymerization solution was diluted with $CHCl_3$ and passed over an alumina (activated neutral) column to remove the catalyst. Solvent was removed by rotary evaporation, and the polymer was isolated by precipitation into hexane.

Molecular weight ($M_n$) and molecular weight distribution ($M_w/M_n$) were determined by GPC equipped with an autosampler (Waters, 717 plus), HPLC pump with THF as eluate at 35 °C and at a flow rate of 1 mL/min (Waters, 515) and four columns (guard, $10^5$ Å, $10^3$ Å, 100 Å; Polymer Standards Services) in series. The GPC was equipped with a differential refractive index detector. Toluene was used as internal standard. Calculations of molar mass were determined using PSS software using a calibration based on linear polystyrene standards. Polymers were analyzed after etching silica with HF, silica 0.5106 mmol Br/1 g silica ~2600 initiating sites per silica particle (on the basis of elementary analysis). Poly(*n*-butyl acrylate) PBA, $M_n$ = 53 500, $M_w/M_n$ = 1.25 and poly(*n*-butyl acrylate-*b*-methyl methacrylate) poly(BA-*b*-MMA), $M_n$ = 104 900, $M_w/M_n$ = 1.28.

Bulk samples of the $SiO_2$-*g*-PBA-*b*-PMMA hybrid were annealed at 160 °C ($T_g$ of PBA ~ −50 °C [40,41], $T_g$ of PMMA ~ 125 °C [31]) for 24 h prior to microtoming for transmission electron microscopy (TEM). Microtoming was performed at room temperature to obtain thin sections ~100 nm in thickness that were used for electron microscopy. TEM imaging was carried out on a JEOL JEM-2010 electron microscope (at the Microscopy & Imaging Center at Texas A&M University, College Station, TX), which was operated at an accelerating voltage of 120 kV under bright-field conventional mode. The TEM images were obtained at a magnification of 50,000×.

TEM was performed on the unstained section, floated onto a Cu-coated grid (obtained from Ted Pella), to determine the arrangement of the $SiO_2$ nanoparticles. Selective staining was also performed on microtomed sections of the hybrids to highlight the structure of the individual blocks in these hybrid materials [31]. For preferential staining of the PMMA block, TEM grids with thin microtomed sections of the hybrid were floated onto 2 wt% aqueous solution of phosphotungstic acid (PTA) and benzyl alcohol (obtained from EMS). The aqueous solution of PTA and benzyl alcohol was at 60 °C, and the TEM grid was floated for 1 min, following a method previously reported in the literature [31]. The TEM grid was next dipped in DI water, to remove excess acid, and dried over lint-free paper. For selectively staining of the PBA block, the hybrid nanocomposite was kept immersed in a 0.5 wt% ruthenium tetraoxide ($RuO_8$, from EMS) solution for 10 days. The stained hybrid nanocomposite was then microtomed, after washing with DI water and drying, and transferred onto the TEM grid.

Atomic Force Microscopy (AFM) was performed on thin films (< 500 nm, and typically ~ 100 nm) of the hybrid cast onto acid-etched Si wafers (to make the wafers hydrophobic and prevent film dewetting off the surface). The thin films were cast from a dilute solution (0.025 wt%) of the hybrid in tetrahydrofuran (THF), which is a good solvent for the PBA-*b*-PMMA diblock copolymer, at a speed of 6000 rpm in a spin-coater. Tapping mode AFM was performed on the thin films, annealed at 160 °C, and both topology and phase contrast images were obtained.

Glass transition temperature ($T_g$) associated with individual blocks of the hybrid nanocomposite was obtained using a PerkinElmer Pyris 1 DSC instrument with sub-ambient capability, at a heating and cooling

rate of 10 °C/min. Data reported here are based on the second heat after an initial heat up to 180 °C [27].

Small-angle neutron scattering (SANS) samples were prepared in a vacuum mold, pressed into a 13 mm diameter pellet under melt conditions, to ensure bubble-free samples. SANS measurements were performed on the 30 m SANS beamline (NG7) at NIST, Gaithersburg, MD. Neutrons with wavelength (λ) of 6 Å and Δλ/λ of 0.15 were used with sample-to-detector distances ranging from 3 to 15.3 m. The SANS data were reduced and corrected for background scattering [42,43]. A q-independent incoherent scattering correction was subtracted prior to data analysis [42]. The SANS data were analyzed using a library of SANS fitting models, in IGOR PRO (Wavemetrics Inc).

Synchrotron SAXS measurements were performed in situ at the beamline X27C, National Synchrotron Light Source (NSLS), Brookhaven National Laboratory (BNL), Upton, NY, using x-rays with wavelength (λ) of 1.371 Å. A one-dimensional linear position-sensitive detector and two-dimensional Mar CCD camera for SAXS were used along with a pinhole collimation system and a temperature controlled sample cell [44,45].

## 3. Results and discussion

The structure of the nanoparticle grafted block copolymer was examined using a combination of electron microscopy, atomic force microscopy and small angle x-ray and neutron scattering (SAXS and SANS, respectively). On the basis of the reported value of the Flory-Huggins interaction parameter of χ for PMMA and PBA that varies from 0.047 at room temperature to 0.03 at 180 °C and considering the molecular weight of the polymers and the near equal volume fractions of PBA and PMMA [31,46], it was anticipated that the blocks should be strongly microphase separated (with ODTs above the degradation temperature of the polymers) in the absence of the silica nanoparticles. The block copolymer, cleaved from the nanoparticles, is microphase separated at all temperatures and exhibits the expected lamellar structure. Differential scanning calorimetry (DSC) revealed the presence of two glass transitions at ~ −50 °C and at ~ +125 °C (Fig. 1), consistent with the values for pure PBA and PMMA respectively, and indicating the presence of a strongly microphase separated block copolymer structure in these $SiO_2$-*g* -(PBA-*b*-PMMA) hybrid materials.

An unstained TEM image of a thin (~100 nm thick) microtomed slice from a previously melt annealed sample ($T_{anneal}$ = 160 °C for 24 h) is shown in Fig. 2. Due to the high electron contrast between the $SiO_2$ nanoparticle and the two polymers, the arrangement of the $SiO_2$ particles can be discerned. Specifically, in contrast to the $SiO_2$-*g*-PBA *parent* hybrid or a 40:60 blend of $SiO_2$-*g*-PBA ($M_n$ = 53 500): PBA ($M_n$ = 55 000) mixture (~the same $SiO_2$ loading) that show FCC ordering of the $SiO_2$ particles (see SAXS data) [18], the $SiO_2$-*g*-(PBA-*b*-PMMA) hybrid exhibits a disordered arrangement of the $SiO_2$ particles in the polymer matrix. We note that the parent SiO2-g-PBA alluded to above was the precursor of the material prior to the co-polymerization of the PMMA block.

In order to examine the arrangement of the individual blocks of the copolymer, each of the blocks was selectively stained using a protocol developed previously by Leibler and coworkers [31]. Specifically, ruthenium tetraoxide ($RuO_4$) was used to selectively stain the PBA block and phosphotungstic acid (PTA) to selectively stain the outer PMMA block and the electron micrographs are presented in Fig. 3. As expected from the synthesis of the hybrids, the PBA block when stained with $RuO_4$, clearly surrounds the silica nanoparticle and further, as would be expected from the random arrangement of the silica particles observed in Fig. 2, demonstrates a random arrangement of the PBA rich domains with respect to each other. Due to concerns of penetration of the dye to the PBA domains (through a glassy PMMA matrix), various conditions of staining conditions – with the exposure from $RuO_4$ ranging from 1 h to 20 days were examined. With the exception of short exposure times where the silica arrangement was recovered, the images obtained were identical in structural features and only varying in intensities. On the other hand, the PTA stained micrograph (Fig. 3b) demonstrates that the outer PMMA block forms a continuous matrix, while the silica particles with the associated PBA inner block form disordered structures of various shapes including individual PBA covered silica particles. Furthermore there is a hint that the silica particles form short contiguous "worm-like chains" with the PBA blocks either in contact or in close

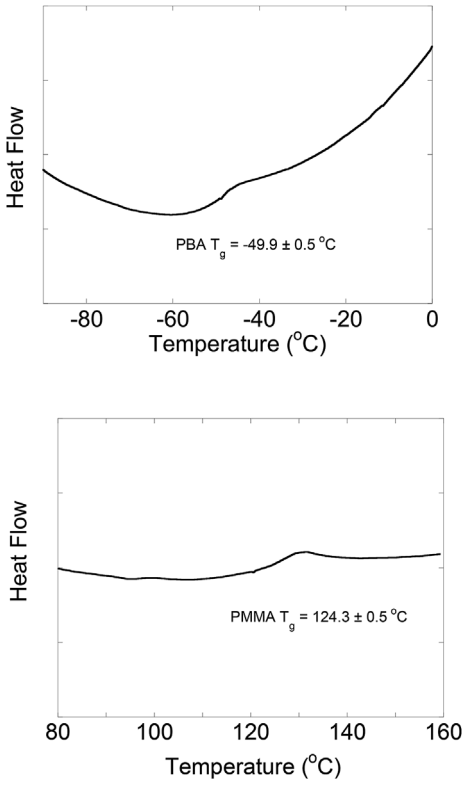


**Fig. 1.** Differential Scanning Calorimetry (DSC) results showing distinct glass transition temperatures ($T_g$) for the two blocks of PBA and PMMA in the diblock chains grafted from the $SiO_2$ nanoparticle. The values of the Tgs are close to those of the pure components and indicate a strongly segregated block copolymer.

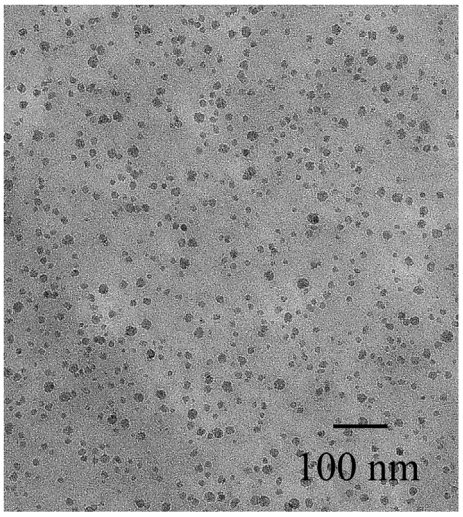


**Fig. 2.** Transmission electron micrograph showing the arrangement of the $SiO_2$-*g*-(PBA-*b* -PMMA) hybrid nanoparticles. The image is taken on an unstained sample, microtomed to ~100 nm in thickness. The sample was annealed at 160 °C for 24 h before microtoming. The micrographs indicate a random dispersion of the $SiO_2$ nanoparticles.

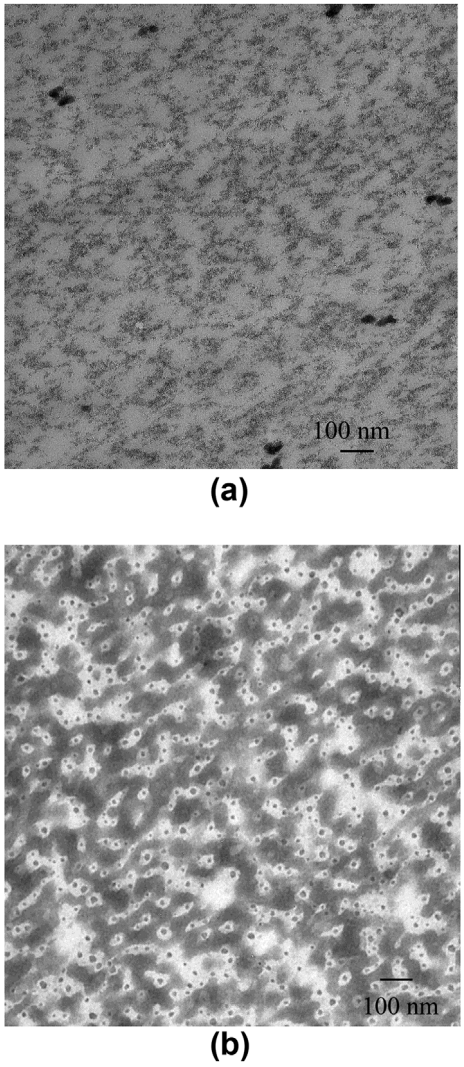


**Fig. 3.** Transmission electron micrograph showing the morphology of the $SiO_2$-*g*-(PBA-*b*-PMMA) hybrid nanocomposite, with selective staining of individual blocks. The thin microtomed section was stained with $RuO_4$ solution, which selectively stains the inner PBA block (Fig. 3a), and with PTA solution, which selectively stains the outer PMMA block (Fig. 3b). The stained regions are observed as darker regions and the unstained regions are observed as lighter regions.

proximity to each other; this conjecture is investigated more thoroughly in this paper through the use of scattering methods. While the staining using PTA occurs much faster than that by $RuO_4$, a similar kinetic study of PTA staining was utilized to rule out artifacts because of excess staining.

While the above morphological study was performed on annealed bulk samples that were microtomed, a similar study on thin films of the block copolymer hybrid prepared by spin-coating from dilute solutions onto silicon wafers or a carbon coated electron microscopy grid and subsequently annealed in the melt state were also performed. Such a solution method for sample preparation in a confined thin film of thickness typically of ~100 nm leads to a similar random ordering of the silica nanoparticles, as observed from a TEM image in Fig. 4a of a sample dropped on a carbon-coated electron microscopy grid and subsequently annealed. Tapping mode atomic force microscopy exploits the mechanical contrast between the hard silica nanoparticles, the soft elastomeric PBA block and the hard glassy properties of the PMMA block. Fig. 4b and c represent the topology and phase angle, respectively, for one such scan on an annealed supported block copolymer

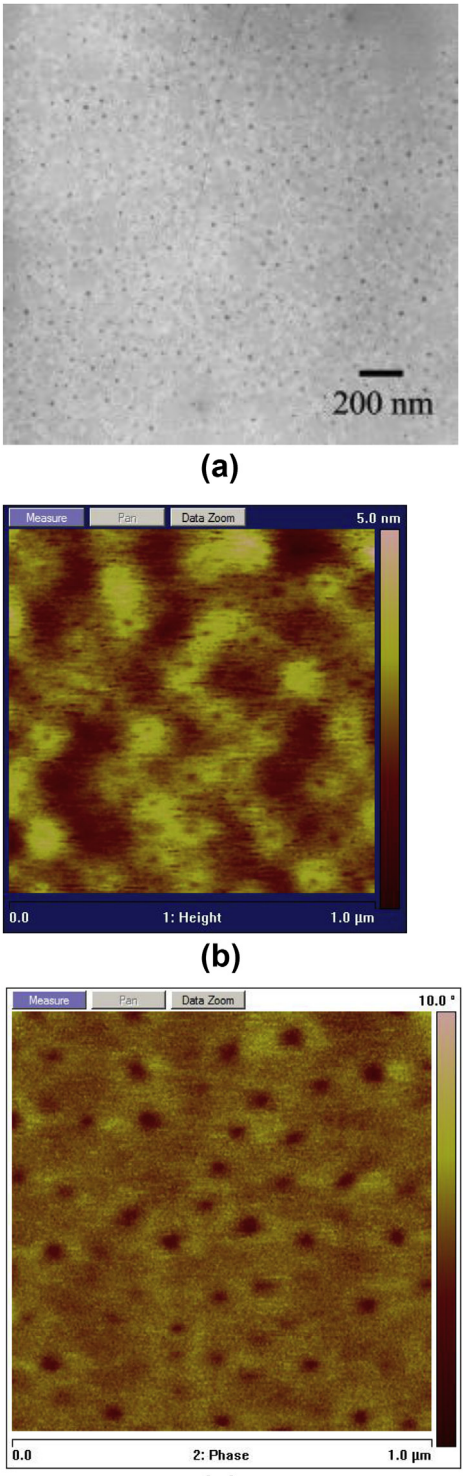


**Fig. 4.** (a) TEM of a thin film, prepared by solvent casting on to a TEM grid followed by annealing at 160 °C that demonstrates the random ordering of the silica nanoparticles. Tapping mode atomic force microscopy, of a thin film of the block copolymer hybrid supported on a silicon wafer with Fig. 4b being the topology and Fig. 4c representing the phase angle. The samples were spin-cast on to a silicon wafer followed by annealing at 160 °C. (For interpretation of the references to colour in this figure legend, the reader is referred to the Web version of this article.)

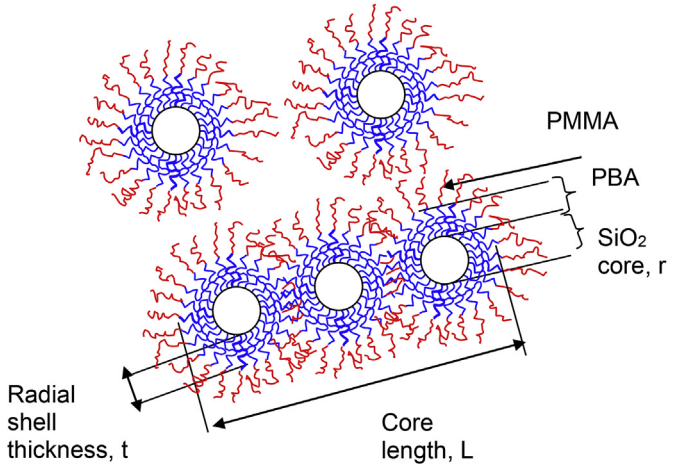


**Fig. 5.** Schematic showing the proposed model for the morphology of the PBA-*b*-PMMA diblock chains tethered to the $SiO_2$ nanoparticles. The model considers the morphology as a combination of a worm-like cylindrical and a spherical core-shell morphology.

thin film. Again, as in the bulk morphology, these thin films are observed to adopt a similar disordered morphology consisting of a combination of individual spherical brush entities and a stringing of a few of these entities to form a short worm-like morphology or perhaps even bicontinuous structures. On the basis of these observations of the bulk and thin films of the $SiO_2$-*g*-(PBA-*b*-PMMA) block copolymer, it could be concluded that the structural arrangement can be summarized as the schematic shown in Fig. 5. We speculate that the co-existence of individual spherical moieties and short worm-like cylindrical objects is perhaps a result of kinetic limitations on the rearrangement of the block copolymer structure on the surface of the nanoparticles to accommodate the worm-like structures. We conjecture that issues such as the dispersity of grafting or block copolymer dispersity (compositional and molecular weight), which are low as prepared, are perhaps not the underlying cause for the observed co-existence. Based on the $SiO_2$-*g*-PBA hybrids and their ability to demonstrate highly ordered structures as recently shown [18], it is assumed that the dispersity of grafting density in the nanoparticle hybrids is minimal and therefore unlikely to cause the disordering behavior observed. Moreover, the molecular weight distribution between the parent PBA homopolymer and the block copolymer of PBA and PMMA are roughly similar suggesting that any additional effects due to the copolymerization are minimal.

To further examine and quantify the structural order of bulk samples SANS measurements that primarily exploit the large scattering contrast between that of the $SiO_2$ and the polymers as a function of temperature were conducted. The neutron scattering length densities at 130 °C for $SiO_2$, PBA and PMMA are $3.2 \times 10^{-6}$, $0.5 \times 10^{-6}$ and $1.0 \times 10^{-6}$ Å$^{-2}$, respectively, and indicates that the contrast between the $SiO_2$ and the polymers is significantly (~a factor of 25) larger than those between the polymeric blocks. SANS intensity data (I(q)) as a function of q for the nanoparticle tethered with hompolymer and nanoparticle tethered with block copolymer are presented in Fig. 6a as a function of temperature. Several features are noteworthy: (a) The q-independent low-angle scattering ($q < 0.006$ Å$^{-1}$) that is distinctly differed for the two cases; (b) With increasing temperature the transition from q-independent to a power-law regime at small angles moves progressively to higher angle; and (c) The presence of a scattering maximum at $q \sim 0.017$ Å$^{-1}$ with I(q) scaling $\sim q^{-4}$ at higher values of q, with the location of the maximum roughly independent of temperature. Similar data were also obtained from SAXS measurements at 30 °C and the data are shown in Fig. 7. In Fig. 7, the SAXS data from the hybrid-diblock to that from the parent $SiO_2$-*g*-PBA homopolymer hybrid were compared [18]. Clearly, the SAX scattering from the diblock and homopolymer (parent $SiO_2$-*g*-PBA) hybrid are significantly different and are consistent with the notion that the arrangement of the silica nanoparticles is distinctly different in the two cases, with the exception of the near similarity of the peak location at ~ 0.017 Å$^{-1}$. For the case of the $SiO_2$-*g*-PBA ($M_n$ = 53 500) hybrid (a precursor of the block copolymer hybrid), clearly two peaks are observed in the scattering. This is attributed to the formation of an FCC lattice of the $SiO_2$ nanoparticles with a lattice spacing of 27 nm. The addition of the PMMA block to this hybrid material led to a significant disordering of the (silica) arrangement and was observed from the considerable broadening of the peak (at 0.017 Å$^{-1}$) and the absence of a second order peak at higher q values.

A combination of individual core-shell spherical objects and worm-like cylinders was used to model the experimental SANS data for the NP tethered homopolymer and NP tethered block copolymer are shown in Fig. 6. While the correlations between the particles dominates the scattering features for the $SiO_2$-*g*- PBA (SAXS data in Fig. 7), it could be recognized that for the case of the block copolymer grafted on to the silica nanoparticles, the structure is significantly disordered, and in the initial analysis the correlations between domains were ignored [23,24]. Further, as demonstrated in the Supporting Information, the scattering data can be fitted to various models with equal efficacy and our choice of fitting is largely driven by the physical insights provided by the direct space microscopy data described previously.

Since the real space images demonstrate the existence of individual spherical moieties, we use a spherical form factor, given as [47]:

$$I(q) = P(q) = \left( \frac{\varphi}{v_m} \frac{3Kv_m}{(qR_m)^3} [\sin(qR_m) - qR_m \cos(qR_m)] \right)^2 \quad (1)$$

where ϕ is the volume fraction of the spherical moieties, K is the scattering contrast between the $SiO_2$ core and the polymer (here taken as the PBA, due to the near equality in the scattering length densities of the PBA and the PMMA blocks), and $R_m$ and $v_m$ are the radius and volume of the spherical moieties respectively.

On the other hand, we use a core-shell cylindrical form factor with the $SiO_2$ nanoparticles at the core, surrounded by a shell of the PBA blocks, in a matrix (considered here as solvent) of PMMA. The scattering intensity is given by Ref. [47]:

$$I(q) = P(q) = \frac{\varphi}{v_m} \int_0^{\pi/2} f^2(q, \alpha) \sin\alpha \; d\alpha$$

$$f(q, \alpha) = 2(\rho_{core} - \rho_{shell}) v_{core} j_0\left(q\frac{L}{2}\cos\alpha\right) \frac{J_1(qr\sin\alpha)}{(qr\sin\alpha)}$$

$$+ 2(\rho_{shell} - \rho_{solvent}) v_{shell} j_0\left(q\left(\frac{L}{2} + t\right)\cos\alpha\right) \frac{J_1(q(r+t)\sin\alpha)}{(q(r+t)\sin\alpha)}$$

$$v_{core} = \pi r^2 L; \quad v_{shell} = \pi(r+t)^2 L_{total}; \quad j_0(x) = \frac{\sin(x)}{x} \quad (2)$$

Where in $J_1$ is the first order Bessel function, the various ρ's are the scattering length densities of the various components, $\phi$ is the volume fraction of cylinders, $r$ is the core radius, $L$ is the cylinder length, $t$ is the shell thickness and $\alpha$ is the angle between the cylinder axis and q. The smeared form of the models were used to account for the wavelength spread of the neutron beam and the smearing associated with SANS experiments [43].

The SANS data were fit to the model described above and the geometrical parameters corresponding to the worm-like cylinder and the spherical core-shell structures were obtained. Attempts to fit the scattering to either of the functional forms independently led to poor fits over the whole q-range over which scattering was measured. The fitting methodology consisted of fitting a low q-range ($0.003$ Å$^{-1}$ $< q <$ $0.01$ Å$^{-1}$) to the core-shell cylindrical form factor, and a high q-range ($0.01$ Å$^{-1}$ $< q <$ $0.05$ Å$^{-1}$) to the core-shell spherical form factor. The fits were performed on the SANS data obtained at different temperatures, after subtracting an incoherent component (typically ~ 1 cm$^{-1}$) that originates primarily from the hydrogen atoms in the scattering volume, and are shown for two

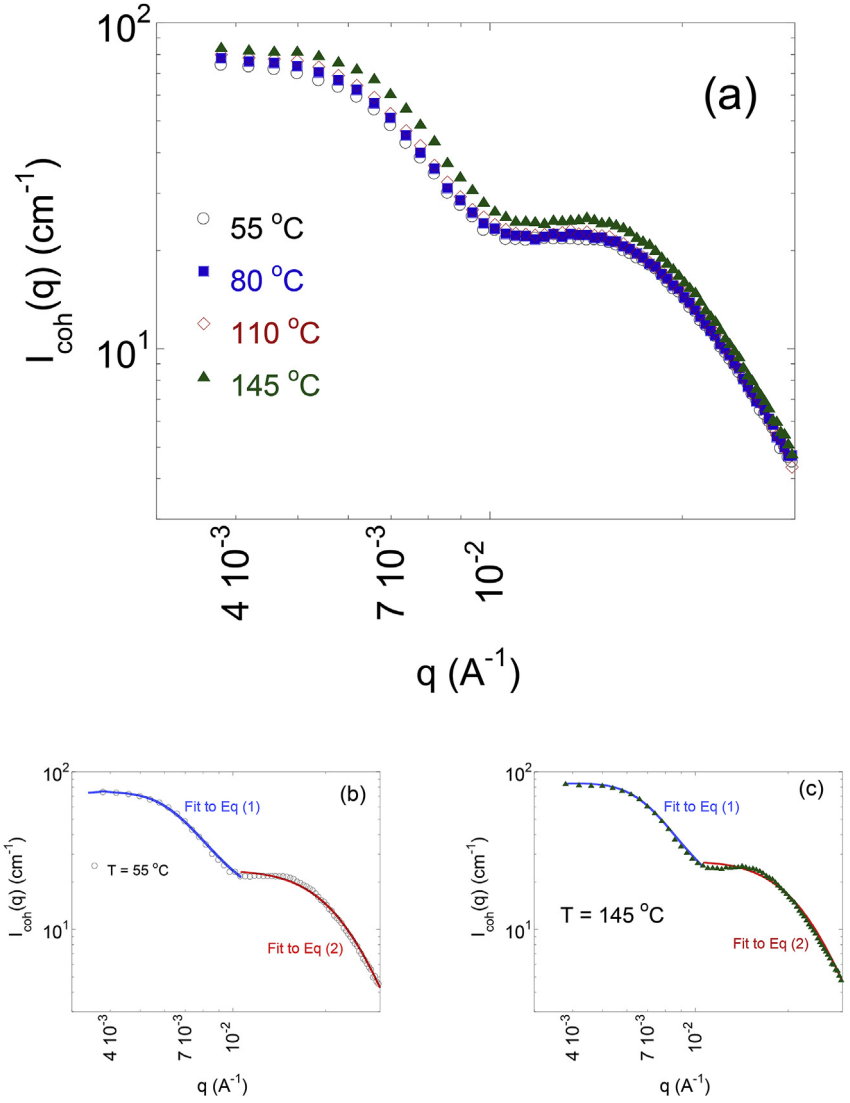


**Fig. 6. (a)** Coherent small angle neutron scattering (SANS) intensities ($I_{coh}(q)$) as a function of wavevector q for the $SiO_2$-*g*-(PBA-*b*-PMMA) hybrid as a function of temperature. The data were fit as described in the text to models described by equations (1) and (2) and the geometrical parameters corresponding to the worm-like cylinders and the individualized core-shell particles extracted. **(b and c)** Fitting of coherent SANS intensity to equations (1) and (2) at T = 55 °C and 145 °C respectively.

temperatures in Fig. 6b and c. In the fitting procedure, the neutron scattering length densities of the constituent components were held constant, and the fit parameters (primarily the shell length, the core radius and the shell thickness) allowed to float and converge to the best solution, under no applied constraints, thereby generating a global optimum. Further, in case of the core-shell spherical form factor, to account for dispersity in the $SiO_2$ nanoparticle size, a Gaussian distribution was assumed. The fits revealed that for the cylindrical morphology, the core radius of the individual spheres was ~13 ± 2 nm, and the shell thickness was ~14 ± 2 nm, and these values were mostly independent of temperature. The total length of the cylinder decreased with increasing temperature, as observed in Fig. 8. The decrease in length of the cylinder is consistent with the decreasing repulsive thermodynamic interactions between PBA and PMMA with increasing temperature combined with the increased dynamics of the PMMA block (at and above the $T_g$ of the PMMA block), leading to perhaps more mixing of the PMMA and PBA blocks at elevated temperatures. On the other hand, for the core-shell spherical particles, however, the morphology is largely independent of temperature, with the core size ~12 ± 2 nm in radius, and a shell thickness of ~12 ± 2 nm.

Clearly the PBA and PMMA chains are strongly incompatible and form microphase separated structure as evidenced by the presence of two glass transitions (close to those of the pure components), the observation of lamellar microphase separated structures when cleaved from the nanoparticle, and the electron and atomic force microscopy results described above. In spite of the fact that the hybrid material only consists of 2% $SiO_2$ by volume, considering the impenetrability of the silica nanoparticles and considering the dimensions of the constituents ($r_{SiO_2}$ ~ 8 nm; $R_{g\ (PBA,Unperturbed)}$ ~ 7 nm and $R_{g\ (PMMA,Unperturbed)}$ ~ 8 nm) it is clear that the $SiO_2$ nanoparticles can indeed perturb the development of the microphase separated morphology. Further, the curvature imposed on the PBA chains, due to the high density of grafting from a relatively small spherical nanoparticle, and the curvature induced on the PBA-*b*-PMMA interface could lead to a significant perturbation from the lamellar structure anticipated for such a block copolymer. Finally, this block copolymer was synthesized by the use of controlled/living radical polymerization methods however does possess a dispersity that is considerably larger than that observed from monodisperse (living anionic polymerization based materials). As shown recently in several studies that have considered the role of dispersity, the phase diagram for block copolymers can be significantly altered because of reduction in chain-stretching experienced by the

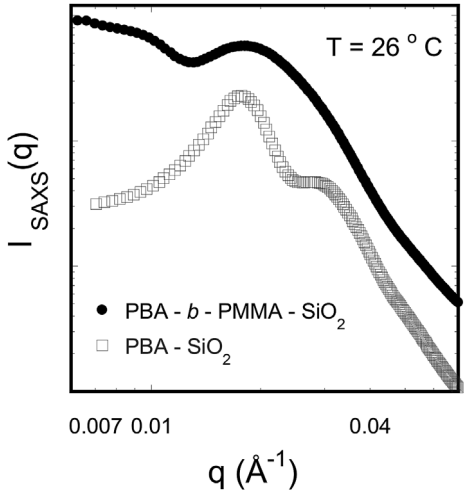


**Fig. 7.** Comparison of the wavevector dependence of small angle x-ray scattering intensity for the parent $SiO_2$-*g*-PBA hybrid and the $SiO_2$-*g*-(PBA-*b*-PMMA) hybrid at room temperature (26 °C). While the PBA homopolymer hybrid ($SiO_2$-g-PBA) exhibits scattering consistent with an FCC arrangement of the silica nanoparticles, the block copolymer hybrid exhibits a combination of worm-like cylinder and randomly distributed individual core-shell structures.

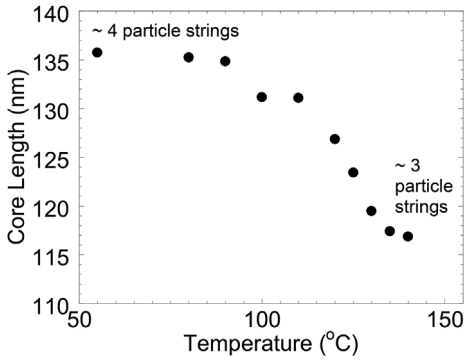


**Fig. 8.** The length of the worm-like cylinders obtained by fitting the temperature dependent SANS data, as described in the text. The cylinder length is the only geometrical parameter that changes significantly with changing temperature and is consistent with the decreasing thermodynamic incompatibility between PBA and PMMA with increasing temperature, with the largest changes occurring near the $T_g$ of the PMMA block.

chains at the microphase separated interface [31,48–53]. It is conceivable that the phase diagram is shifted to form cylindrical microdomains with the PBA chains forming the inner core and the PMMA forming the matrix [48,50].

On the other hand, the formation of highly ordered and hexagonally arranged cylinders is possibly prevented by the curvature imposed by the tethering of the PBA chains to the silica nanoparticles and therefore forcing not only the curvature but also influencing the number density of the polymer chains and the chain stretching required at the interface, as illustrated by Milner in pioneering theoretical work [54] and by Hadjichristidis et al. using experiments on miktoarm stars [55–58] where they studied the formation of microphase separated structures in star block copolymers. It is noteworthy that the junction point for the inner block PBA chains corresponds to a finite sized nanoparticle unlike the case of star polymers, which terminate at a point, and leads to significant imposition of the particle curvature on the PBA-*b*-PMMA interface. Thus, it can be expected that the PBA and PMMA chains at the interface would experience different chain stretching and therefore prevent the formation of flat interfaces. Clearly, such a situation in the case of the $SiO_2$-*g*-(PBA-*b*-PMMA) would significantly decrease the chain stretching penalties at the PBA – PMMA interface and therefore allow for the formation of curved interfaces as observed experimentally here. Finally, with increasing temperature, however, the incompatibility between PBA and PMMA decreases, due to the decrease in $\chi$ with increasing temperature [31], and this results in the shortening of the average cylinder length and more individual hybrid particles in a PMMA matrix.

## 4. Concluding remarks

We have demonstrated in this paper that the ordering and arrangement of microphase-separating block copolymers when tethered to a spherical nanoparticle is significantly altered from their bulk analogs. Using a combination of microscopy techniques and small angle scattering methods, we have shown that the high grafting density along with the relatively small radius of the spherical nanoparticle imposes a curvature on the block copolymer, that it adopts a combination of individual core-shell moieties along with worm-like cylinders, with a string of about 3–5 $SiO_2$ nanoparticles forming the core of the cylinder. Clearly, understanding the role of changing chain length along with composition of the block, grafting density, size of nanoparticle and the relative placement of the polymeric blocks with respect to the nanoparticle is the first step towards truly understanding the effect of nanoparticles on such block copolymer behavior. Further understanding the effect of tethering the block copolymer to a nanoparticle on the interfacial behavior of such a system (in a polymer blend, for example) would be extremely interesting to pursue. Additionally, understanding the wetability and interpenetration of homopolymers [25] in such block copolymer hybrids would certainly be interesting.

## Acknowledgements

VG and RK gratefully acknowledge the support of the National Science Foundation (CMMI-0708096). JP and KM thank the National Science Center, Poland (via Grant UMO-2014/14/A/ST5/00204, and DEC-2012/04/M/ST5/00805) and the National Science Foundation (DMR-05-49353) for their financial support. This work utilized neutron scattering facilities supported in by the National Science Foundation, USA (NSF) under Agreement No. DMR-0454672. We thank Dr. Zhiping Luo of the Microscopy and Imaging Center, Texas A&M University (TEM), Dr. Guoting Qin for help with the AFM measurementsy and Dr. Carlos Avila Orta, Dr. Igor Sics and Dr. Raj Somani for help at the NSLS at Brookhaven National Laboratory (X27C).

## Appendix A. Supplementary data

Supplementary data to this article can be found online at https://doi.org/10.1016/j.polymer.2018.10.072.

## References

[1] J.P. Koski, A.L. Frischlmecht, Fluctuation effects on the brush structure of mixed brush nanoparticles in solution, ACS Nano 12 (2) (2018) 1664–1672.
[2] M. Elsabahy, K.L. Wooley, Strategies toward well-defined polymer nanoparticles inspired by nature: chemistry versus versatility, J. Polym. Sci., Polym. Chem. Ed. 50 (10) (2012) 1869–1880.
[3] H.K. Chao, R.A. Riggleman, Inverse design of grafted nanoparticles for targeted self-assembly, Mole. Syst. Desig. Eng. 3 (1) (2018) 214–222.
[4] S.F. Cheng, M.J. Stevens, G.S. Grest, Ordering nanoparticles with polymer brushes, J. Chem. Phys. 147 (22) (2017).
[5] S.K. Kumar, V. Ganesan, R.A. Riggleman, Perspective: outstanding theoretical questions in polymer-nanoparticle hybrids, J. Chem. Phys. 147 (2) (2017).
[6] M. Asai, D. Zhao, S.K. Kumar, Role of grafting mechanism on the polymer coverage and self-assembly of hairy nanoparticles, ACS Nano 11 (7) (2017) 7028–7035.
[7] K.J. Modica, T.B. Martin, A. Jayaraman, Effect of polymer architecture on the structure and interactions of polymer grafted particles: theory and simulations, Macromolecules 50 (12) (2017) 4854–4866.
[8] B.J. Kim, J. Bang, C.J. Hawker, E.J. Kramer, Effect of areal chain density on the location of polymer-modified gold nanoparticles in a block copolymer template, Macromolecules 39 (12) (2006) 4108–4114.
[9] B.J. Kim, J.J. Chiu, G.R. Yi, D.J. Pine, E.J. Kramer, Nanoparticle-induced phase

transitions in diblock-copolymer films, Adv. Mater. 17 (21) (2005) 2618–+.
[10] P. Chmielarz, J.J. Yan, P. Krys, Y. Wang, Z.Y. Wang, M.R. Bockstaller, K. Matyjaszewski, Synthesis of nanoparticle copolymer brushes via surface-initiated seATRP, Macromolecules 50 (11) (2017) 4151–4159.
[11] T.B. Martin, A. Seifpour, A. Jayaraman, Assembly of copolymer functionalized nanoparticles: a Monte Carlo simulation study, Soft Matter 7 (13) (2011) 5952–5964.
[12] E.R. Chan, L.C. Ho, S.C. Glotzer, Computer simulations of block copolymer tethered nanoparticle self-assembly, J. Chem. Phys. 125 (6) (2006).
[13] C.L. Phillips, C.R. Iacovella, S.C. Glotzer, Stability of the double gyroid phase to nanoparticle polydispersity in polymer-tethered nanosphere systems, Soft Matter 6 (8) (2010) 1693–1703.
[14] C.L. Yi, S.Y. Zhang, K.T. Webb, Z.H. Nie, Anisotropic self-assembly of hairy inorganic nanoparticles, Accounts Chem. Res. 50 (1) (2017) 12–21.
[15] J.Y. Zhang, P.J. Santos, P.A. Gabrys, S. Lee, C. Liu, R.J. Macfarlane, Self-assembling nanocomposite tectons, J. Am. Chem. Soc. 138 (50) (2016) 16228–16231.
[16] J. Che, K. Park, C.A. Grabowski, A. Jawaid, J. Kelley, H. Koerner, R.A. Vaia, Preparation of ordered monolayers of polymer grafted nanoparticles: impact of architecture, concentration, and substrate surface energy, Macromolecules 49 (5) (2016) 1834–1847.
[17] T.B. Martin, C. McKinney, A. Jayaraman, Effect of blockiness in grafted monomer sequences on assembly of copolymer grafted nanoparticles: a Monte Carlo simulation study, Soft Matter 9 (1) (2013) 155–169.
[18] V. Goel, J. Pietrasik, H.C. Dong, J. Sharma, K. Matyjaszewski, R. Krishnamoorti, Structure of polymer tethered highly grafted nanoparticles, Macromolecules 44 (20) (2011) 8129–8135.
[19] A.S. Silva, C.A. Mitchell, M.F. Tse, H.C. Wang, R. Krishnamoorti, Templating of cylindrical and spherical block copolymer microdomains by layered silicates, J. Chem. Phys. 115 (15) (2001) 7166–7174.
[20] R. Krishnamoorti, A.S. Silva, C.A. Mitchell, Effect of silicate layer anisotropy on cylindrical and spherical microdomain ordering in block copolymer nanocomposites, J. Chem. Phys. 115 (15) (2001) 7175–7181.
[21] A. Jayaraman, K.S. Schweizer, Effective interactions and self-assembly of hybrid polymer grafted nanoparticles in a homopolymer matrix, Macromolecules 42 (21) (2009) 8423–8434.
[22] V. Goel, J. Pietrasik, K. Matyjaszewski, R. Krishnamoorti, Linear viscoelasticity of polymer tethered highly grafted nanoparticles, in: K. Matyjasewski (Ed.), Controlled/living Radical Polymerization: Progress in Atrp, 2009, pp. 257–267.
[23] A.T. Lorenzo, R. Ponnapati, T. Chatterjee, R. Krishnamoorti, Structural characterization of aqueous solution poly(oligo(ethylene oxide)monomethyl methacrylate)-grafted silica nanoparticles, Faraday Discuss 186 (2016) 311–324.
[24] Y. Jiao, P. Akcora, Understanding the role of grafted polystyrene chain conformation in assembly of magnetic nanoparticles, Phys. Rev. 90 (4) (2014).
[25] T.B. Martin, K.I.S. Mongcopa, R. Ashkar, P. Butler, R. Krishnamoorti, A. Jayaraman, Wetting-dewetting and dispersion aggregation transitions are distinct for polymer grafted nanoparticles in chemically dissimilar polymer matrix, J. Am. Chem. Soc. 137 (33) (2015) 10624–10631.
[26] J. Pyun, T. Kowalewski, K. Matyjaszewski, Synthesis of polymer brushes using atom transfer radical polymerization, Macromol. Rapid Commun. 24 (2003) 1043–1059.
[27] V. Goel, T. Chatterjee, L. Bombalski, K. Yurekli, K. Matyjaszewski, R. Krishnamoorti, Viscoelastic properties of silica-grafted poly(styrene-acrylonitrile) nanocomposites, J. Polym. Sci. B Polym. Phys. 44 (14) (2006) 2014–2023.
[28] J.-S. Wang, K. Matyjaszewski, Controlled/"living" radical polymerization. atom transfer radical polymerization in the presence of transition-metal complexes, J. Am. Chem. Soc. 117 (20) (1995) 5614–5615.
[29] K. Matyjaszewski, J. Xia, Atom transfer radical polymerization, Chem. Rev. 101 (9) (2001) 2921–2990.
[30] N.V. Tsarevsky, K. Matyjaszewski, "Green" atom transfer radical polymerization: from process design to preparation of well-defined environmentally friendly polymeric materials, Chem. Rev. 107 (6) (2007) 2270–2299.
[31] A.-V. Ruzette, S. Tence-Girault, L. Leibler, F. Chauvin, D. Bertin, O. Guerret, P. Gerard, Molecular disorder and mesoscopic order in polydisperse acrylic block copolymers prepared by controlled radical polymerization, Macromolecules 39 (17) (2006) 5804–5814.
[32] L. Leibler, Theory of microphase separation in block copolymers, Macromolecules 13 (1980) 1602–1617.
[33] M.A. Modi, R. Krishnamoorti, M.F. Tse, H.-C. Wang, Viscoelastic characterization of an order–order transition in a mixture of di- and triblock copolymers, Macromolecules 32 (10) (1999) 4088–4097.
[34] J. Xia, K. Matyjaszewski, Controlled/"Living" radical polymerization. Atom transfer radical polymerization catalyzed by copper(I) and picolylamine complexes, Macromolecules 32 (8) (1999) 2434–2437.
[35] W. Jakubowski, K. Matyjaszewski, Activator generated by electron transfer for atom transfer radical polymerization, Macromolecules 38 (10) (2005) 4139–4146.
[36] W. Jakubowski, K. Min, K. Matyjaszewski, Activators regenerated by electron transfer for atom transfer radical polymerization of styrene, Macromolecules 39 (1) (2006) 39–45.
[37] K. Min, H. Gao, K. Matyjaszewski, Preparation of homopolymers and block copolymers in miniemulsion by ATRP using activators generated by electron transfer (AGET), J. Am. Chem. Soc. 127 (11) (2005) 3825–3830.
[38] K. Matyjaszewski, H. Dong, W. Jakubowski, J. Pietrasik, A. Kusumo, Grafting from surfaces for "everyone": ARGET ATRP in the presence of air, Langmuir 23 (8) (2007) 4528–4531.
[39] L. Bombalski, K. Min, H. Dong, C. Tang, K. Matyjaszewski, Preparation of well-defined hybrid materials by ATRP in miniemulsion, Macromolecules 40 (21) (2007) 7429–7432.
[40] T. Hayakawa, K. Adachi, Miscibility of poly(n-butyl acrylate)/poly(propylene glycol) blends. 1. Phase behavior and dielectric relaxation, Macromolecules 33 (2000) 6834–6839.
[41] D.A. Savin, J. Pyun, G.D. Patterson, T. Kowalewski, K. Matyjaszewski, Synthesis and characterization of silica-graft-polystyrene hybrid nanoparticles: effect of constraint on the glass-transition temperature of spherical polymer brushes, J. Polym. Sci. B Polym. Phys. 40 (2002) 2667–2676.
[42] R. Krishnamoorti, W.W. Graessley, N.P. Balsara, D.J. Lohse, J. Chem. Phys. 100 (1994) 3894.
[43] S.R. Kline, Reduction and analysis of SANS and USANS data using IGOR Pro, J. Appl. Crystallogr. 39 (2006) 895–900.
[44] T. Chatterjee, C.A. Mitchell, V.G. Hadjiev, R. Krishnamoorti, Hierarchical polymer-nanotube composites, Adv. Mater. 19 (22) (2007) 3850–+.
[45] C.A. Mitchell, R. Krishnamoorti, Dispersion of single-walled carbon nanotubes in poly(epsilon-caprolactone), Macromolecules 40 (5) (2007) 1538–1545.
[46] W. Sriprom, M. James, S. Perrier, C. Neto, Ordered microphase separation in thin films of PMMA-PBA synthesized by RAFT: effect of block polydispersity, Macromolecules 42 (8) (2009) 3138–3146.
[47] K. Yurekli, C.A. Mitchell, R. Krishnamoorti, Small-angle neutron scattering from surfactant-assisted aqueous dispersions of carbon nanotubes, J. Am. Chem. Soc. 126 (2004) 9902–9903.
[48] M.W. Matsen, Polydispersity-induced macrophase separation in diblock copolymer melts, Phys. Rev. Lett. 99 (14) (2007).
[49] A.J. Meuler, C.J. Ellison, C.M. Evans, M.A. Hillmyer, F.S. Bates, Polydispersity-driven transition from the orthorhombic Fddd network to lamellae in poly(isoprene-b-styrene-b-ethylene oxide) triblock terpolymers, Macromolecules 40 (20) (2007) 7072–7074.
[50] M.W. Matsen, Effect of large degrees of polydispersity on strongly segregated block copolymers, Eur. Phys. J. E 21 (3) (2006) 199–207.
[51] R.B. Thompson, M.W. Matsen, Improving polymeric microemulsions with block copolymer polydispersity, Phys. Rev. Lett. 85 (3) (2000) 670–673.
[52] A.V. Dobrynin, L. Leibler, Theory of polydisperse multiblock copolymers, Macromolecules 30 (16) (1997) 4756–4765.
[53] H. Tanaka, S. Sakurai, T. Hashimoto, M.D. Whitmore, Elastic-scattering from asymmetric, polydisperse block copolymer systems in the disordered state, Polymer 33 (5) (1992) 1006–1013.
[54] S.T. Milner, Chain architecture and asymmetry in copolymer microphases, Macromolecules 27 (8) (1994) 2333–2335.
[55] G. Floudas, S. Pispas, N. Hadjichristidis, T. Pakula, I. Erukhimovich, Microphase separation in star block copolymers of styrene and isoprene. Theory, experiment, and simulation, Macromolecules 29 (11) (1996) 4142–4154.
[56] S. Pispas, Y. Poulos, N. Hadjichristidis, Micellization behavior of (PS)(8)(PI)(8) miktoarm (Vergina) star copolymers, Macromolecules 31 (13) (1998) 4177–4181.
[57] G. Floudas, T. Pakula, G. Velis, S. Sioula, N. Hadjichristidis, Equilibrium order-to-disorder transition temperature in block copolymers, J. Chem. Phys. 108 (15) (1998) 6498–6501.
[58] S. Pispas, A. Avgeropoulos, N. Hadjichristidis, J. Roovers, Hydrodynamic properties of A(8)B(8) type miktoarm (Vergina) stars, J. Polym. Sci. B Polym. Phys. 37 (12) (1999) 1329–1335.